

## RNA 5-methylcytosine status is associated with DNMT2/TRDMT1 nuclear localization in osteosarcoma cell lines

Gabriela Betlej<sup>a,1</sup>, Tomasz Ząbek<sup>b,1</sup>, Anna Lewińska<sup>c</sup>, Dominika Błoniarczyk<sup>c,\*</sup>, Iwona Rzeszutek<sup>c,\*</sup>, Maciej Wnuk<sup>c,\*</sup>

<sup>a</sup> Institute of Physical Culture Studies, College of Medical Sciences, University of Rzeszow, Rzeszow 35-310, Poland

<sup>b</sup> Laboratory of Genomics, National Research Institute of Animal Production, Krakowska 1, Balice 32-083, Poland

<sup>c</sup> Department of Biotechnology, Institute of Biology and Biotechnology, College of Nature Sciences, University of Rzeszow, Pigoń 1, Rzeszow 35-310, Poland

### ARTICLE INFO

#### Keywords:

Osteosarcoma  
TRDMT1  
RNA 5-methylcytosine  
DNA damage response  
Telomere maintenance  
Redox homeostasis

### ABSTRACT

Osteosarcoma (OS) is a pediatric malignant bone tumor with unsatisfying improvements in survival rates due to limited understanding of OS biology and potentially druggable targets. The present study aims to better characterize osteosarcoma U-2 OS, SaOS-2, and MG-63 cell lines that are commonly used as *in vitro* models of OS. We focused on evaluating the differences in cell death pathways, redox equilibrium, the activity of proliferation-related signaling pathways, DNA damage response, telomere maintenance, DNMT2/TRDMT1-based responses and RNA 5-methylcytosine status. SaOS-2 cells were characterized by higher levels of superoxide and nitric oxide that promoted AKT and ERK1/2 activation thus modulating cell death pathways. OS cell lines also differed in the levels and localization of DNA repair regulator DNMT2/TRDMT1. SaOS-2 cells possessed the lowest levels of total, cytoplasmic and nuclear DNMT2/TRDMT1, whereas in MG-63 cells, the highest levels of nuclear DNMT2/TRDMT1 were associated with the most pronounced status of RNA 5-methylcytosine. *In silico* analysis revealed potential phosphorylation sites at DNMT2/TRDMT1 that may be related to the regulation of DNMT2/TRDMT1 localization. We postulate that redox homeostasis, proliferation-related pathways and DNMT2/TRDMT1-based effects can be modulated as a part of anti-osteosarcoma strategy reflecting diverse phenotypic features of OS cells.

### 1. Introduction

Osteosarcoma (OS) is the most common primary bone tumor affecting mostly children and adolescents [1]. The annual rate of global OS incidence is 3.4 per million people and the 5-year survival rate is 60–70% [2,3]. OS is highly metastatic and has a high risk of recurrence after treatment [4]. Development of OS has been associated with the mutations of tumor suppressors, such as *TP53*, *RB1*, *REQL4*, and *INK4a* and/or deregulation of PI3K/mTOR, RANKL/NF-κB, TGFβ, and IGF pathways [5]. However, agents targeting these pathways have not achieved successful clinical outcomes [5]. The heterogeneous profile, the unbalanced karyotype, and changes in immune dynamics make conventional treatment regimens of OS less efficient [6–8]. Therefore, it is important to understand the mechanisms underlying the development of OS to find new alternative molecular approaches for early diagnosis and therapy.

For *in vitro* studies of OS, U-2 OS, SaOS-2, and MG-63 cell lines are frequently used as experimental models [9–11]. These are one of the most popularly available OS cancer cell lines that share many similarities [12], hence providing a platform for parallel comparisons. Despite the well-known similarities, there are, however, differences between these cell lines. For example, U-2 OS, SaOS-2, and MG-63 cells possess a different degree of differentiation [13]. SaOS-2 cells show rather a mature phenotype, while U-2 OS cell line is negative for almost all osteoblastic markers. Interestingly, MG-63 cells have the most heterogeneous profile, as they possess both mature and immature osteoblastic features [13]. Additionally, U-2 OS cells are positive for cartilage marker, collagen IV type, which is only expressed in very early differentiation stages but not by mature osteoblasts [13]. Therefore, U-2 OS cells are frequently classified as fibroblastic [14,15]. Moreover, the large panel of OS cell lines was genetically described [16] and proteome comparison of U-2 OS and SaOS-2 cells has been performed [17]. The

\* Corresponding authors.

E-mail addresses: [irzeszutek@ur.edu.pl](mailto:irzeszutek@ur.edu.pl) (I. Rzeszutek), [mwnuk@ur.edu.pl](mailto:mwnuk@ur.edu.pl) (M. Wnuk).

<sup>1</sup> These authors are first co-authors.

comparative studies revealed 89 up-regulated and 86 down-regulated proteins in SaOS-2 cells compared to U-2 OS cells [17].

Furthermore, these cell lines are used as a reference model in studies that aim to develop new drugs, find druggable targets and gain insight into drug metabolism [11,18–21]. Recently, anticancer epigenetic drugs targeting RNA methylation are becoming a hot topic in cancer research, including OS [22–24]. Interestingly, it has been shown that knockout (KO) of *DNMT2/TRDMT1* gene (encoding tRNA-aspartic acid methyltransferase 1) compromised homologous recombination (HR) process and prevented drug resistance in OS cells [25,26]. Moreover, our previous studies have shown that U-2 OS cells lacking *DNMT2/TRDMT1* gene exhibit changes in DDR mechanism, telomere length, retrotransposon activity, and IFN- $\beta$ -mediated response leading to cellular and genetic heterogeneity that modulate cancer cell responses to chemotherapy [27]. These new findings indicate a pivotal role of TRDMT1 in OS therapy, motivating us to investigate TRDMT1-mediated RNA m<sup>5</sup>C modification in other OS cell lines. Moreover, the comparative studies of DNMT2/TRDMT1-based response and the differences in the activity of signaling pathways between U-2 OS, SaOS-2 and MG-63 cells have not yet been revealed. Identifying the differences between these cell lines may help to understand the diverse and even opposite outcomes in response to the same pharmacological treatment. Moreover, specific determination of the traits of U-2 OS, SaOS-2, and MG-63 cells can give a hint, which of the cell line is the most relevant to predicting efficient treatment in the clinic.

In this study, we evaluated selected phenotypic features of three osteosarcoma cell lines, namely U-2 OS, SaOS-2 and MG-63 cells and focused on cell death pathways, redox status, the activity of proliferation-associated pathways, DNA damage response, DNMT2/TRDMT1 methyltransferase-based effects and RNA 5-methylcytosine status. We documented that redox disequilibrium may promote sustained AKT and ERK1/2 activation thus affecting cell death pathways in OS cells. Furthermore, nuclear TRDMT1 levels may be associated with the status of RNA 5-methylcytosine that may be considered as a novel molecular marker for predicting therapy response in OS patients.

## 2. Materials and methods

### 2.1. Cell lines and culture conditions

Experiments were performed on osteosarcoma cell lines: U-2 OS (92022711, ECACC, Public Health England, Porton Down, Salisbury, UK), MG-63 (86051601, ECACC, Public Health England, Porton Down, Salisbury, UK), and SaOS-2 (89050205, ECACC, Public Health England, Porton Down, Salisbury, UK). Cells were grown at 37 °C in DMEM medium supplemented with 10% (v/v) FBS and 100 U/ml penicillin, 0.1 mg/ml streptomycin, and 0.25  $\mu$ g/ml amphotericin B (Corning, Tewksbury, MA, USA) in the presence of 5% CO<sub>2</sub>.

### 2.2. Apoptosis

Phosphatidylserine externalization (an apoptotic biomarker) was evaluated using Muse® Cell Analyzer and Muse® Annexin V and Dead Cell Assay Kit following the manufacturer's instructions (Luminex Corporation, Austin, TX, USA). Representative dot plots are shown.

### 2.3. Oxidative stress

Changes in intracellular superoxide levels were analyzed using Muse® Cell Analyzer and Muse® Oxidative Stress Kit (Luminex Corporation, Austin, TX, USA) as previously described [23]. Briefly, superoxide-positive and superoxide-negative subpopulations were determined. Representative histograms (%) are presented.

### 2.4. Nitric oxide levels

Nitric oxide levels were evaluated using Muse® Cell Analyzer and Muse® Nitric Oxide Kit (Luminex Corporation, Austin, TX, USA) as described elsewhere [28]. Briefly, nitric oxide specific fluorogenic probe DAX-J2<sup>TM</sup> orange and a death marker, 7-aminoactinomycin D (7-AAD) were used to discriminate between the production of nitric oxide in live (7-AAD-negative) and dead (7-AAD-positive) cells. Representative dot plots are presented.

### 2.5. ERK1/2 and Akt activity

Extracellular signal-regulated kinase 1/2 (ERK1/2) and Akt activity was evaluated using Muse® Cell Analyzer and Muse® PI3K/MAPK Dual Pathway Activation Kit using two directly conjugated antibodies, anti-phospho-Akt (Ser473)-Alexa Fluor TM 555 and anti-phospho-ERK1/2 (Thr202/Tyr204, Thr185/Tyr187) conjugated antibody-PECy5 according to the manufacturer's instructions (Luminex Corporation, Austin, TX, USA). Representative dot plots are shown.

### 2.6. DNA damage response (DDR)

The phosphorylation status of ATM and H2AX was assessed using Muse® Cell Analyzer and Muse® Multi-Color DNA Damage kit according to the manufacturer's instructions (Luminex Corporation, Austin, TX, USA). The activation of ATM and H2AX was studied using a phospho-specific ATM (Ser1981)-PE and phospho-specific histone H2AX-PECy5 conjugated antibodies. Four cell subpopulations were revealed using flow cytometry analysis, namely pATM(-) and pH2AX(-) cells (no DNA damage), pATM(+) and pH2AX(-) cells (ATM activation), pATM(-) and pH2AX(+) cells (H2AX activation) and pATM(+) and pH2AX(+) cells (dual activation of ATM and H2AX – cells with DSBs).

### 2.7. Western blot

The cell protein extracts were prepared according to [29]. The following primary and secondary antibodies were used: anti-DNMT2/TRDMT1 (A-7, sc-271513, 1:500), anti-RAD51 (MA5-14419, 1:200), anti-RAD52 (MA5-31888, 1:500), anti-XRCC1 (MA5-12071, 1:500) and horseradish peroxidase (HRP)-conjugated secondary antibody (7076, 1:3000, Thermo Fisher Scientific, Waltham, MA, USA). The chemiluminescent HRP substrate was purchased from BioRad (Clarity<sup>TM</sup> Western ECL Blotting Substrate). Images were acquired using a G:BOX imaging system (Syngene, Cambridge, UK). Densitometry measurements of the bands were performed using ImageJ software (<https://imagej.nih.gov/ij/>, U. S. National Institutes of Health, Bethesda, MD, USA) and the mean value out of at least two independent experiments is shown. The data represent the relative density compared to  $\beta$ -actin (A3854, Merck KGaA, Darmstadt, Germany, 1:40 000).

### 2.8. Telomere FISH assay

Telomere length was evaluated using Telomere PNA FISH Kit/Cy3 (Dako, Glostrup, Denmark) according to the manufacturer's instructions with some modifications. Telomere length was analyzed using flow cytometry (Amnis® FlowSight®, Luminex Corporation, Austin, TX, USA) and appropriate software (IDEAS version 6.2.187.0, Luminex Corporation, Austin, TX, USA).

### 2.9. Immunofluorescence

An immunostaining protocol was used as previously described [23]. Fixed cells were incubated with the primary antibodies, anti-DNMT2/TRDMT1 (D-9, 1:100, sc-365001, Santa Cruz Biotechnology, Dallas, TX, USA), anti-NSUN2 (1:250, 702036, Thermo Fisher Scientific, Waltham, MA, USA), anti-TRF1 (1:250, NB100-1701, Novus Biologicals,

Littleton, CO, USA), anti-TRF2 (1:300, ab108997, Abcam, Cambridge, UK), anti-lamin A/C (1:100, MA3-1000, Thermo Fisher Scientific, Waltham, MA, USA) and anti-lamin B1 (1:500, PA5-19468, Thermo Fisher Scientific, Waltham, MA, USA) at 4 °C overnight. Next, secondary antibodies conjugated to Texas Red (1:1000, T2767) or FITC (1:1000, F2761) (Thermo Fisher Scientific, Waltham, MA, USA) were used at room temperature for 1 h. Nuclei were visualized using Hoechst 33342 staining. Cell images were acquired using a laser-based confocal imaging and high-content analysis (HCA) system IN Cell Analyzer 6500 HS (Cytiva, Marlborough, MA, USA). Quantitative analysis was performed using IN Carta software (Cytiva, Marlborough, MA, USA). The immunofluorescent signals of the proteins analyzed (protein levels) are presented as relative fluorescence units (RFU).

For TRF1, TRF2, lamin A/C and lamin B1 studies, DNA was visualized using PI staining. Fluorescent immuno-signals were captured using Amnis® FlowSight® imaging flow cytometer (Luminex Corporation, Austin, TX, USA). To evaluate the levels of TRF1, TRF2, lamin A/C and lamin B1, IDEAS software version 6.2.187.0 (Luminex Corporation, Austin, TX, USA) was used.

### 2.10. RNA methylation

RNA methylation, namely the levels of 5-methylcytosine (5-mC), was analyzed using dedicated ELISA-based assay MethylFlash 5-mC RNA Methylation ELISA Easy Kit (P-9009-96, EpiGentek, Farmingdale, NY, USA) according to the manufacturer's instructions.

### 2.11. PCR amplification and Sanger sequencing of DNMT2/TRDMT1 mRNA isoforms

2000 ng of total RNA were reverse transcribed using Transcriptor First Strand cDNA Synthesis Kit (Roche, Mannheim, Germany). The PCR assay encompassed amplification of eight fragments covering the DNMT2/TRDMT1 mRNA reference sequence of four isoforms (Table S1). Two pairs of PCR primers for each of four isoforms (Fig. S1) were designed using the Primer3 software [30,31] and synthesized by Thermo Fisher Scientific (Waltham, MA, USA). Amplification was performed using hot start Taq DNA polymerase (Qiagen, Hilden, Germany). After an initial step of 95 °C for 15 min, a touchdown PCR procedure (TDPCR) was applied. The initial TDPCR stage included 12 steps of annealing temperature decreases of 1.0 °C in the range from 67 °C down to 56 °C. The second stage of TDPCR included 30 PCR cycles with annealing at 55 °C. Each cycle of amplification included 30 s of denaturation at 94 °C, 1 min of annealing, and 30 s of extension at 72 °C. Amplification was ended with the final extension step at 72 °C for 7 min. PCR amplifications were performed on the VeritiPro Thermal Cycler (Thermo Fisher Scientific, Waltham, MA, USA). Amplified cDNA samples were run in two percent agarose gel stained with ethidium bromide for the evaluation of the quality of amplified cDNAs. PCR products were sequenced using PCR primers and the BigDye™ Terminator v3.1 Cycle Sequencing Kit (Thermo Fisher Scientific, Waltham, MA, USA). The manufacturer-recommended cycle sequencing program was applied with the primer annealing of 59 °C and 4 min of extension at 60 °C. Sequencing of PCR products was performed on the VeritiPro Thermal Cycler (Thermo Fisher Scientific, Waltham, MA, USA). Sequencing products were cleaned with the BigDye XTerminator™ Purification Kit (Thermo Fisher Scientific, Waltham, MA, USA) and electrophoresed on the ABI3500xl genetic analyzer (Thermo Fisher Scientific, Waltham, MA, USA).

Obtained sequencing traces were evaluated for quality and subjected to variant genotyping using FinchTV 1.4.0 (Geospiza Inc. Seattle, WA, USA). Further investigations included trace sequence alignment against reference sequences using GENEDOC software [32] to check for the variation among investigated cDNA samples. Obtained sequence traces were also aligned against a reference sequence of the human genome using the blastx option of the NCBI website to check for their homology to the translated sequences encoding DNMT2/TRDMT1 protein

isoforms. GENEDOC software was used for cDNA sequence translation of reported variants of DNMT2/TRDMT1 mRNA.

### 2.12. In silico analysis of potential DNMT2/TRDMT1 post-translational modifications

To test possible post-translational modifications of DNMT2/TRDMT1 freely available computational tool Scansite 4.0 (<http://scansite.mit.edu>) was used. The Scansite program uses scores calculated from position-specific score matrices (PSSM) to search for motifs. The settings of high stringency were selected. The high stringency setting is the most restrictive and reports the motif identified in the query sequence that falls within the top 0.2% of all matching sequences contained in the vertebrate subset of SwissProt proteins. DNMT2/TRDMT1 amino acid sequence was obtained from Uniprot (<https://www.uniprot.org/>), accession number O14717.

### 2.13. Statistical analysis

The results represent the mean ± SD of at least three independent experiments. Box and whisker plots with median, lowest, and highest values were also used. Statistical analysis was performed using the GraphPad Prism 8 software. Comparison between U-2 OS, SaOS-2 and MG-63 cell lines were performed with one-way ANOVA followed by Dunnett's test. Differences between SaOS-2 and MG-63 cells were revealed using one-way ANOVA and Tukey's multiple comparison test. The differences in RNA methylation between all three cell lines were assessed using Student's *t*-test. *P* < 0.05 was considered statistically significant.

## 3. Results and discussion

### 3.1. Comparison of the activity of proliferation-related signaling pathways in U-2 OS, SaOS-2, and MG-63 cells

The *in vitro* cancer model is a major tool to understand the molecular basis of cancer biology for appropriate selection of potential anticancer agents and the investigation of their effectiveness. Thus, it is essential to provide comprehensive characterization of widely used cancer cell lines. In the present study, three osteosarcoma (OS) cell lines, namely U-2 OS, SaOS-2, and MG-63 cells, were compared in terms of cell death pathways, redox homeostasis, the activity of selected proliferation-associated signaling pathways, DNA damage response, telomere maintenance and DNMT2/TRDMT1-based responses that might be potentially important for improving existing and developing new anticancer strategies.

Chemotherapy-induced apoptosis is widely used anticancer approach, however, cancer cells can differently respond to apoptotic stimuli and acquire resistance to chemotherapeutic agents [33]. Therefore, we first compared the susceptibility to apoptotic and necrotic cell death of three OS cell lines in standard growth conditions (Fig. 1A). Slight but statistically significant differences in apoptotic and necrotic parameters were noticed (Fig. 1A, *p* < 0.01, *p* < 0.001). MG-63 cells were the least prone to apoptotic cell death compared to U-2 OS and SaOS-2 cells (Fig. 1A, *p* < 0.01). In contrast, SaOS-2 cells were the most susceptible to necrotic cell death compared to other OS cells (Fig. 1A, *p* < 0.001).

Cancer cells are characterized by elevated production of reactive oxygen species (ROS) mainly due to increased metabolic rates [34]. The role of ROS in cancer biology is rather complex [35,36]. A moderate increase in ROS levels has been shown to promote pro-tumorigenic signaling, enhance tumor development and progression, drive DNA damage and genome instability, and modulate drug resistance [34,37]. However, ROS are also capable of triggering programmed cell death by activating signaling pathways and modulation of oxidative stress is considered as an anticancer strategy [34,37–39]. As different

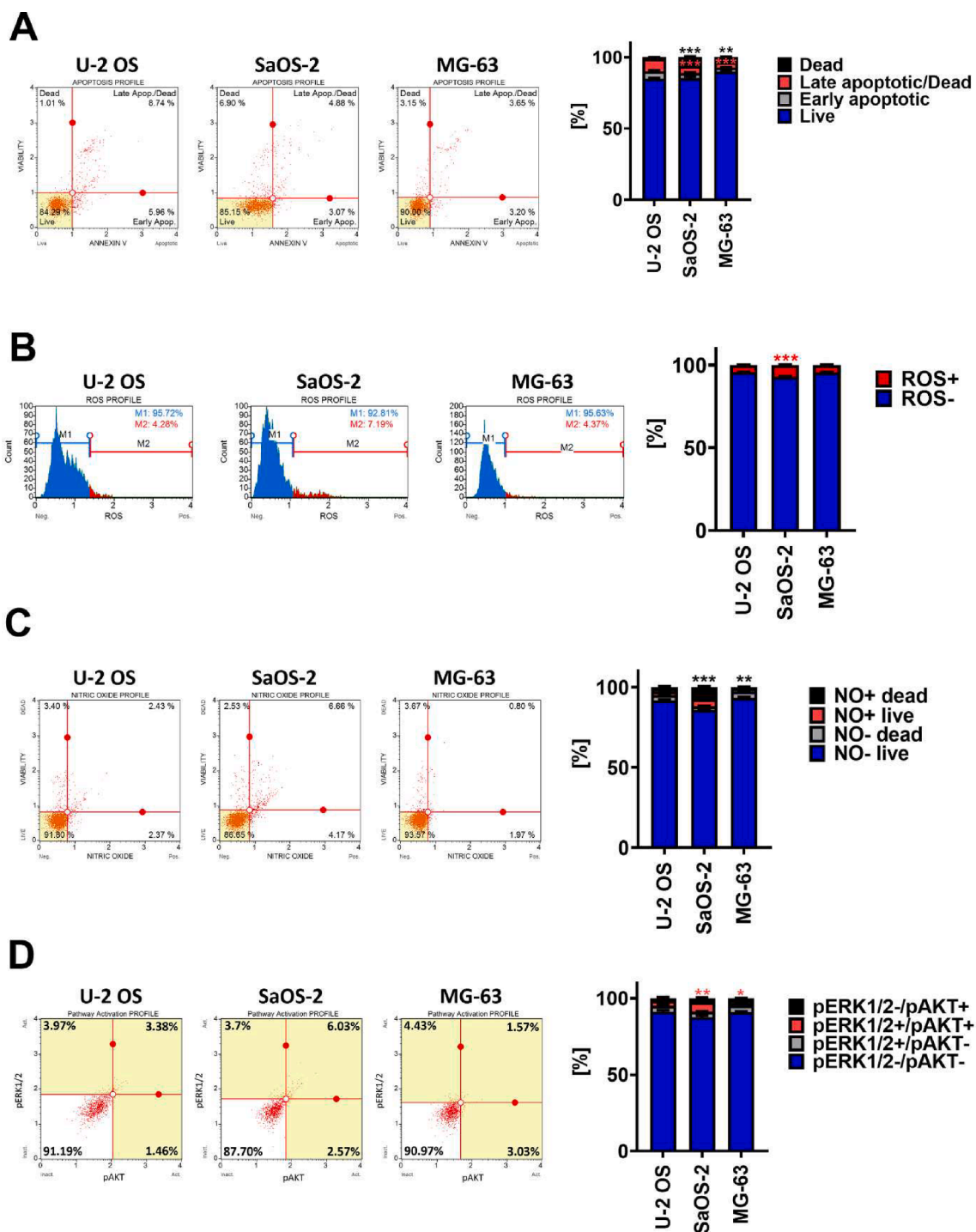


**Fig. 1.** Differences in the (A) apoptotic and necrotic markers, (B) reactive oxygen species (C) and nitric oxide levels as well as (D) AKT and ERK1/2 activity between U-2 OS, SaOS-2 and MG-63 cells. (A) Apoptosis was studied using Annexin V staining and flow cytometry. Representative dot plots are shown. Bars indicate SD,  $n = 3$ ,  $^{**}p < 0.01$ ,  $^{***}p < 0.001$  compared to U-2 OS cells (ANOVA and Dunnett's a posteriori test). Black color of asterix corresponds to necrotic cells. Red color of asterix corresponds to late apoptotic/dead cells. (B) Superoxide levels were evaluated using dihydroethidium (DHE) staining and flow cytometry. Two subpopulations were considered and analyzed [%], namely superoxide-negative subpopulation (blue) and superoxide-positive subpopulation (red). Representative histograms are shown. Bars indicate SD,  $n = 3$ ,  $^{**}p < 0.01$ ,  $^{***}p < 0.001$  compared to U-2 OS cells (ANOVA and Dunnett's a posteriori test). Red color of asterix corresponds to superoxide-positive cell subpopulation. (C) Nitric oxide levels were analyzed using an DAX-J2<sup>TM</sup> orange probe and flow cytometry. Representative dot plots are shown. Bars indicate SD,  $n = 3$ ,  $^{**}p < 0.01$ ,  $^{***}p < 0.001$  compared to U-2 OS cells (ANOVA and Dunnett's a posteriori test). Black color of asterix corresponds to dead cell subpopulation that produces nitric oxide. (D) ERK1/2 and AKT activity (phosphorylation status) was analyzed using Muse<sup>®</sup> Cell Analyzer. Representative dot plots are shown. Bars indicate SD,  $n = 3$ ,  $^{*}p < 0.05$ ,  $^{**}p < 0.01$  compared to U-2 OS cells (ANOVA and Dunnett's a posteriori test). Red color of asterix corresponds to dual activation of ERK1/2 and AKT pathways.

susceptibility to cell death was documented in three OS cell lines (Fig. 1A), we were interested then to analyze if this observation can be related to diverse rates of superoxide production (Fig. 1B). Indeed, a slight but statistically significant difference in ROS production in SaOS-2 cells compared to U-2 OS and MG-63 cells (Fig. 1B,  $p < 0.001$ ) can reflect

the susceptibility of SaOS-2 cells to necrotic cell death (Fig. 1A).

Next, we have focused on the analysis of nitric oxide (NO<sup>•</sup>) levels as elevated pools of nitric oxide are commonly observed in cancer cells [40]. However, NO<sup>•</sup> may also have a role in sensitizing the cancer cells to chemotherapeutic treatment [41]. SaOS-2 cells were characterized by

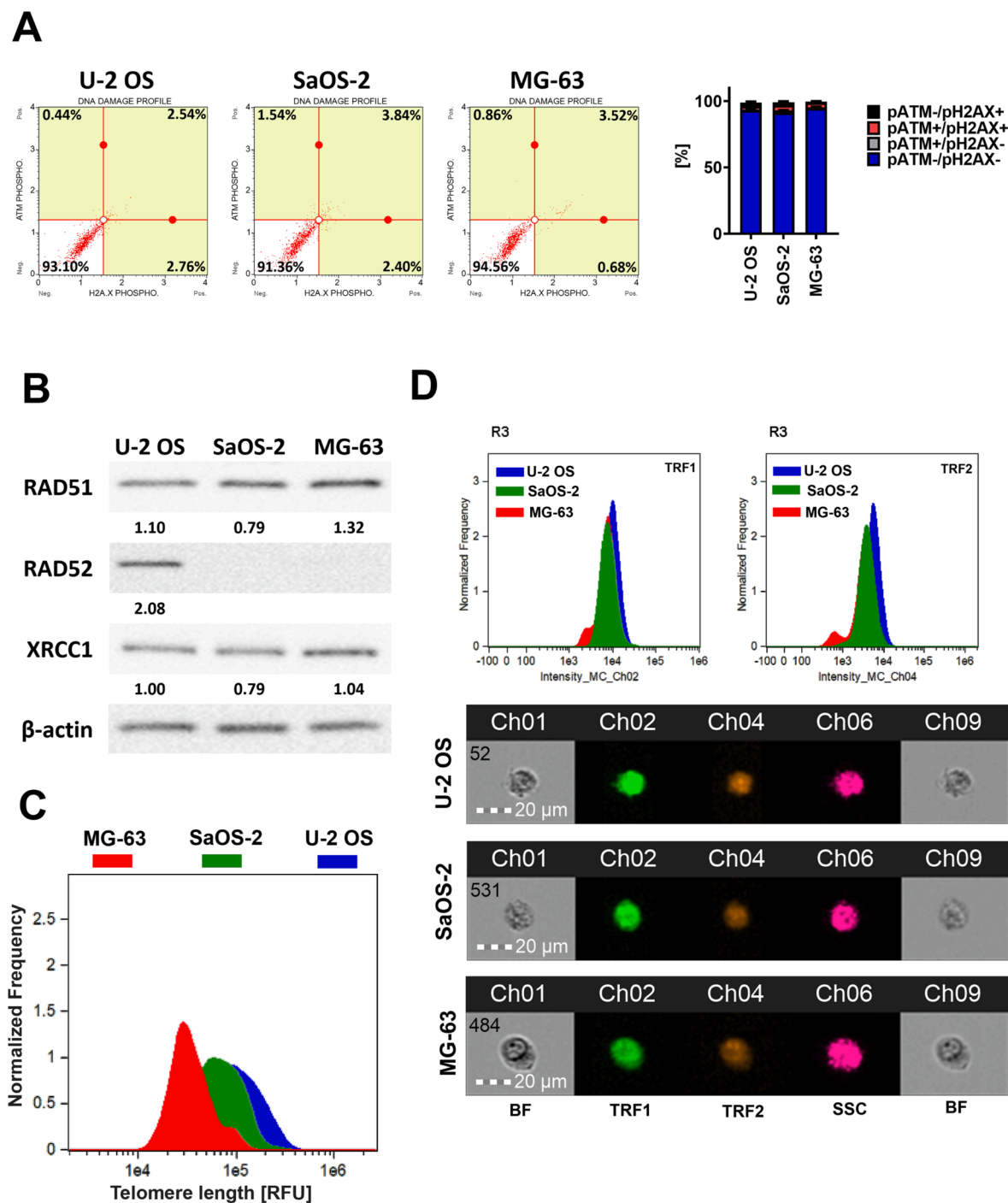


**Fig. 2.** Comparison of DNA damage response (DDR) (A, B), telomere length (C) and TRF1 and TRF2 levels (D) between U-2 OS, SaOS-2 and MG-63 cells. (A) The phosphorylation status of ATM and H2AX was assessed using flow cytometry. Representative dot plots are shown. Bars indicate SD,  $n = 5$ . (B) Western blot-based analysis of the levels of proteins involved in DNA repair. Anti- $\beta$ -actin antibody served as a loading control. Data were normalized to  $\beta$ -actin. (C) Changes in the telomere length were analyzed using imaging flow cytometry. Representative histograms are shown. The red histogram indicates telomere length in MG-63 cells, the green histogram indicates telomere length in SaOS-2 cells, while the blue histogram indicates telomere length in U-2 OS cells. A shift to the right side of the histogram indicates cell subpopulation with longer telomeres. (D) Changes in the levels of TRF1 (left) and TRF2 (right). TRF1 and TRF2 signals were analyzed using immunofluorescence and imaging flow cytometry. Representative histograms are shown (top). The blue histograms indicate TRF1 and TRF2 levels in U-2 OS cells, the green histograms indicate TRF1 and TRF2 levels in SaOS-2 cells, while the red histograms indicate TRF1 and TRF2 levels in MG-63 cells. Representative microphotographs are also shown (bottom). BF- bright field, SSC- side scatter.

the highest levels of nitric oxide compared to other OS cells (Fig. 1C,  $p < 0.001$ ) that can be also correlated with the highest levels of superoxide (Fig. 1B) and the susceptibility to necrotic cell death (Fig. 1A).

ROS may modulate proliferation-related signaling pathways such as PI3K/AKT and extracellular signal-regulated kinase (ERK) pathways [42–44]. Dysregulation of PI3K/AKT pathway has been associated with pathological processes of OS, including proliferation and invasion, cell cycle progression, apoptosis, angiogenesis, metastasis, and chemoresistance [45]. Similar as PI3K/AKT, ERK1/2 pathway was related to proliferation [46], apoptosis [47] and metastasis [48]. Therefore, we analyzed then the levels of phosphorylated forms of AKT and ERK1/2 in three OS cell lines (Fig. 1D). SaOS-2 cells were characterized by slightly higher levels of both phospho-AKT and phospho-ERK1/2 compared to other OS cells (Fig. 1D,  $p < 0.01$ ). Our data are in agreement with the study showing that the PI3K-AKT-mTOR pathway could also be a pro-death signal, especially in the context of necrotic cell death [49,50]. Moreover, it has been shown that ERK activation potentiated cisplatin-induced cell death in SaOS-2 cells [51].

Overall, this may suggest that ROS and NO<sup>\*</sup> production in SaOS-2 cells may promote sustained AKT and ERK1/2 activation thus affecting cell death pathways. Interestingly, SaOS-2 cells have previously been suggested to be more resistant to chemotherapy than other OS cell lines [52]. Therefore, the use of oxidative stress-induced drugs and NO<sup>\*</sup> donors could be a possible strategy to sensitize SaOS-2 cells to chemotherapy-associated cell death.

### 3.2. Differences in the DNA damage response (DDR) in OS cell lines

Genomic instability, a consequence of defective DNA repair pathways or misregulated cell-cycle checkpoints, is one of enabling characteristics of cancer cells [53,54]. The components of DDR can be considered as druggable targets in anticancer strategies [55]. Therefore, we checked the differences in the DDR between OS cell lines. Our analysis indicated very slight differences in ATM activation and dual ATM and  $\gamma$ H2AX activation in SaOS-2 compared to other OS cells (Fig. 2A).

We evaluated then the differences in the expression of selected factors involved in DNA repair mechanism, namely the levels of RAD51, RAD52, and XRCC1 proteins. Interestingly, RAD51 gene knockdown (KD) has been shown to sensitize OS cells to chemo- and radiotherapy [56], while RAD52 is involved in mitotic repair synthesis at telomeres [57]. Chen *et al.* have reported that U-2 OS-TRE cells lacking TRDMT1 gene impairs the localization of RAD51 and RAD52 to the sites of ROS-induced DNA damage [25]. Moreover, our previous studies have shown that treatment with etoposide caused changes in the RAD51 and RAD52 expression levels in U-2 OS cells with DNMT2/TRDMT1 gene KO sensitizing them to the drug treatment [27]. Based on our analysis, the protein levels of RAD51 and XRCC1 were comparable in three OS cell lines (Fig. 2B). Interestingly, RAD52 is expressed in the U-2 OS cell line, whereas no expression of RAD52 was noticed in MG-63 and SaOS-2 cell lines (Fig. 2B). Our analysis is in contrast with the previous studies showing the presence of RAD52 in SaOS-2 and MG-63 cells at the low levels [58].

Telomeres prevent chromosome ends from inducing DNA damage and end-to-end fusion that results in rearrangements [59]. Although the length of the telomere is commonly maintained by telomerase, cancer cells also employ a recombination-based mechanism known as alternative lengthening of the telomeres (ALT) [59]. Of the OS cell lines studied, U-2 OS and SaOS-2 have been characterized as ALT-positive [60,61], while MG-63 as telomerase-positive and ALT-negative [62,63]. Since many DNA repair proteins, including RAD52, have been implicated in the ALT mechanism [57,58], the lack of RAD52 expression in SaOS-2 cells seems to be surprising (Fig. 2B). As the OS cell lines use distinct mechanisms to maintain the telomeres, we evaluated the differences in their telomere length. Based on flow cytometry, we could indicate that the involvement of different mechanisms leads to

differences in telomere length in OS cell lines (Fig. 2C). Our data are in agreement with the Southern blot-based studies showing following telomere length ranking U-2 OS cells (13.7 kbp) > SaOS-2 cells (7.6 kbp) > MG-63 cells (5.8 kbp) [64].

A growing body of evidence suggest that HR process cooperates with components of the shelterin complex [65]. The activity of RAD52 and other HR factors, together with shelterin components TRF2 and TIN2 are required for telomeric D-loop formation [65]. TRF1 and TRF2 are two out of six shelterin complex components and participate in both telomerase-dependent telomere maintenance and ALT mechanism [66,67]. Additionally, binding by TRF1 and TRF2 is essential to protect telomeres against DDR and DNA repair factors [68]. Therefore, we compared then the expression of TRF1 and TRF2 between OS cells. Based on our analysis, we observed a slightly higher expression of TRF1 and TRF2 in U-2 OS cells compared to SaOS-2 and MG-63 cells (Fig. 2D).

### 3.3. The nuclear levels of DNMT2/TRDMT1 methyltransferase are associated with the RNA 5-methylcytosine modification status

RNA methylation in cancer progression has become increasingly prominent. RNA methylation occurs most often at the C5 position of cytosine (RNA:m<sup>5</sup>C) [69]. RNA:m<sup>5</sup>C is regulated by m<sup>5</sup>C-methyltransferases, namely tRNA-specific methyltransferase (DNMT2/TRDMT1) family members and NOL1/NOP2/SUN domain (NSUN) family members. NSUN methyltransferases include several members, namely NSUN1-NSUN7 [70,71]. Out of all NSUN members, NSUN2 possesses the most prominent role in cancer progression [72]. Similarly to NSUN2, DNMT2/TRDMT1 is a multifunctional enzyme that participates in the regulation of cancer cell proliferation, migration, and DDR [23,25,27,73]. Furthermore, the dysregulation of the modification is closely related to human tumor malignancies [74]. Although, RNA:m<sup>5</sup>C plays a crucial role in the diagnosis and prognosis of numerous cancers [75–78], our understanding of the regulation and function of RNA 5-methylcytosine (RNA:m<sup>5</sup>C) modification in OS remains limited. Therefore, we first evaluated the protein levels of DNMT2/TRDMT1 in three OS cell lines (Fig. 3A). Western blot analysis indicated the highest levels of DNMT2/TRDMT1 protein in U-2 OS cells and the lowest levels in SaOS-2 cells, respectively (Fig. 3A).

Since DNMT2/TRDMT1 can be located both in cytoplasmic and nuclear compartments [79–81], we have then investigated the differences in the cytoplasmic and nuclear pools of DNMT2/TRDMT1 between U-2 OS, SaOS-2 and MG-63 cells. Based on our analysis, MG-63 cells were characterized by the highest levels of nuclear DNMT2/TRDMT1 compared to other OS cells (Fig. 3B,  $p < 0.001$ ). U-2 OS cells with the highest total levels of DNMT2/TRDMT1 (Fig. 3A) were also characterized by the highest levels of cytoplasmic fraction of DNMT2/TRDMT1 compared to other OS cells (Fig. 3B). SaOS-2 cells, with the lowest levels of total DNMT2/TRDMT1 (Fig. 3A), possessed also the lowest levels of cytoplasmic and nuclear DNMT2/TRDMT1 (Fig. 3B,  $p < 0.001$ ). Additionally, we evaluated the nuclear and cytoplasmic fractions of NSUN2 (Fig. 3B). SaOS-2 cells were characterized by the lowest levels of cytoplasmic and nuclear NSUN2 compared to other OS cells (Fig. 3B).

Next, we have evaluated the differences in the levels of 5-methylcytosine in RNA of OS cell lines (Fig. 3C). The highest methylation status was observed in MG-63 cells, whereas the lowest levels of 5-methylcytosine were noticed in SaOS-2 cells (Fig. 3C,  $p < 0.001$ ).

Interestingly, it has been previously shown that DNMT2/TRDMT1 may confer resistance to anticancer therapy [25,26]. Therefore, the levels of DNMT2/TRDMT1 can be considered as a novel predictive marker of anticancer drug response, especially in the context of genotoxic drugs.

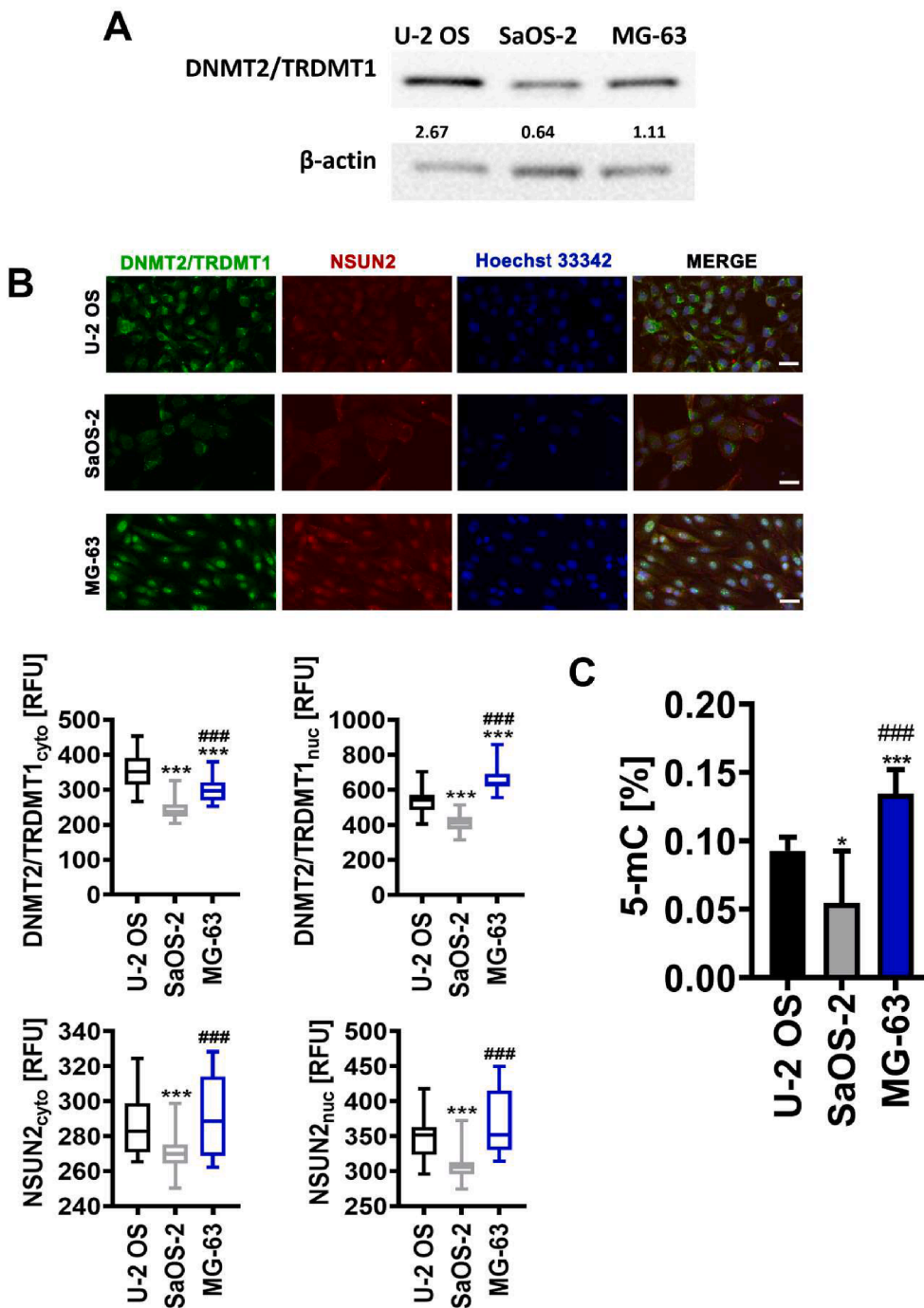


**Fig. 3.** Comparative study of DNMT2/TRDMT1 levels (A), DNMT2/TRDMT1 and NSUN2 localization (B) and 5mC methylation status in RNA (C) in U-2 OS, SaOS-2 and MG-63 cells. (A) Western blot-based analysis of protein levels of DNMT2/TRDMT1. Anti- $\beta$ -actin antibody served as a loading control. Data were normalized to  $\beta$ -actin. (B) Immunofluorescence-based analysis of DNMT2/TRDMT1 (top) and NSUN2 (bottom) cytoplasmic (left) and nuclear (right) fractions. Box and whisker plots are shown,  $n = 3$ ,  $***p < 0.001$  compared to U-2 OS cells (ANOVA and Dunnett's a posteriori test),  $###p < 0.001$  SaOS-2 cells compared to MG-63 cells (ANOVA and Tukey's a posteriori test). Representative immunofluorescent staining of DNMT2/TRDMT1 (green channel) and NSUN2 (red channel) are shown above the boxes. Nuclei were stained with Hoechst 33342. Scale bar – 10  $\mu$ m. (C) ELISA-based analysis of RNA:m<sup>5</sup>C methylation levels [%]. Box and whisker plots are shown,  $n = 3$ ,  $*p < 0.05$ ,  $***p < 0.001$  compared to U-2 OS cells and  $###p < 0.001$  SaOS-2 cells compared to MG-63 cells (Student's *t*-test).

### 3.4. Changes in the DNMT2/TRDMT1 localization may be mediated by post-translational modifications

As the localization of DNMT2/TRDMT1 significantly differs between the cell lines studied, we have next tried to determine the reason for this diversity. It has been previously shown that DNMT2/TRDMT1, which is typically present in nucleus, relocalized to the cytoplasm under stress conditions [82]. Therefore, we check whether this is due to the impaired nuclear architecture that may affect nucleus function. The association between higher lamin B1 expression levels and nuclear dysmorphisms in OS cell lines has been already suggested [83]. Moreover, it has been shown that lamin A interacts with the m<sup>6</sup>A methyltransferases, METTL3 and METTL14 in nuclear speckles [84]. Therefore, we evaluated the differences in the levels of lamin A/C and lamin B1. However, our

analysis indicated that SaOS-2 and MG-63 cells (with the lowest and highest levels of nuclear DNMT2/TRDMT1, respectively) possess similar levels of lamin A/C and lamin B1, which is also higher than in U-2 OS cells (Fig. 4A).

Since alternative splicing results in multiple transcript variants encoding different DNMT2/TRDMT1 isoforms (based on <https://www.uniprot.org/uniprot/O14717>), we tested whether the different DNMT2/TRDMT1 isoforms may show distinct localization patterns. Our analysis, based on sequence alignment including variant A (accession number NM\_004412) of DNMT2/TRDMT1 mRNA and cDNA samples amplified using primers specific to four isoforms (D, E, F and G), showed no differences (Fig. S2). Furthermore, we performed a protein sequence alignment showing the homology of the tested samples at amino acid levels without differences as well (Fig. S3).

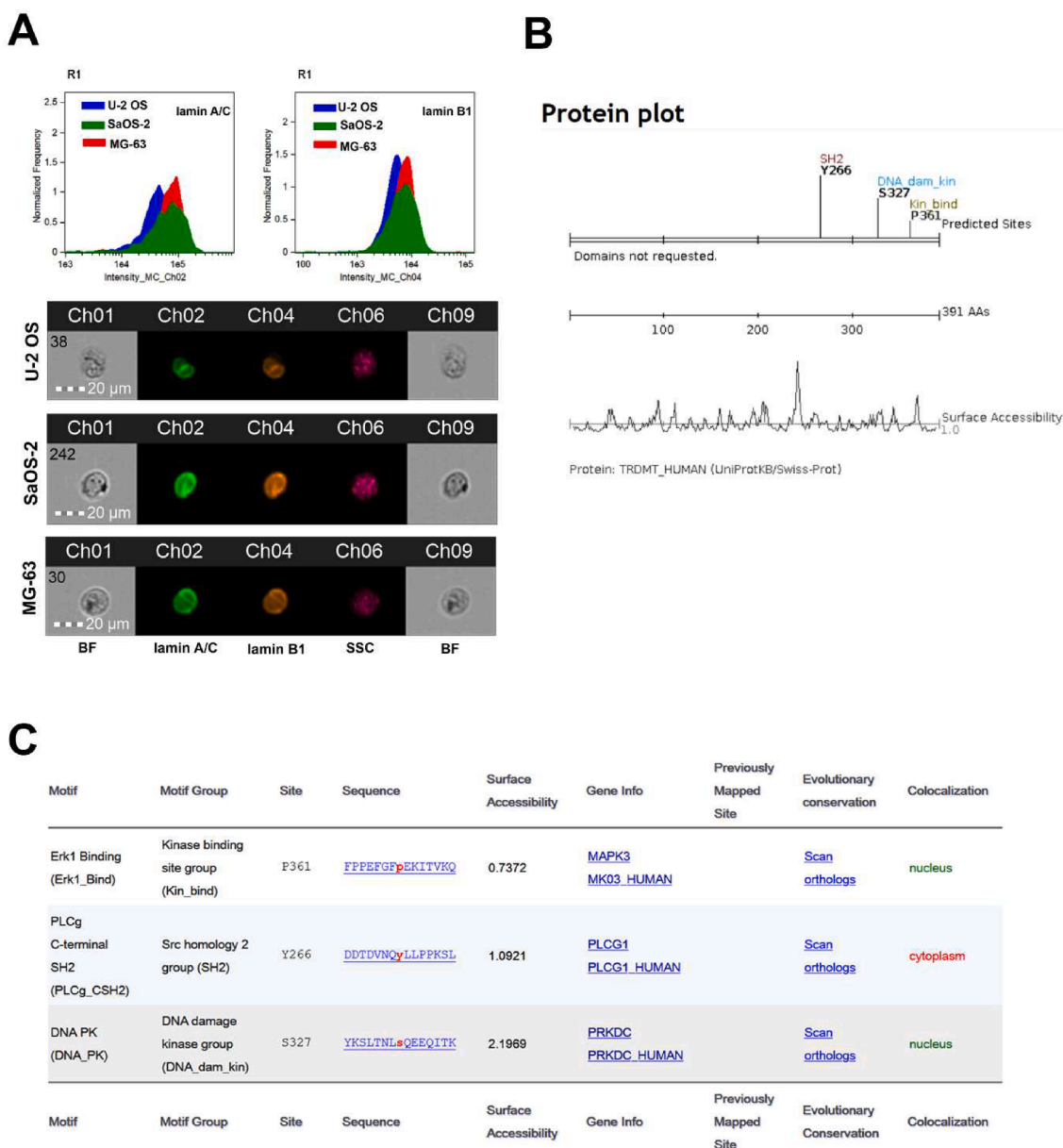


**Fig. 4.** Characterization of the lamin A/C and lamin B1 levels in U-2 OS, SaOS-2 and MG-63 cells (A) and prediction of the post-translational modifications of DNMT2/TRDMT1 (B, C). (A) Changes in the levels of lamin A/C (left) and lamin B1 (right). Lamin A/C and lamin B1 signals were analyzed using immunofluorescence and imaging flow cytometry. Representative histograms are shown (top). The blue histograms indicate lamin A/C and lamin B1 levels in U-2 OS, green histograms indicate lamin A/C and lamin B1 levels in SaOS-2 cells, while red histograms indicate lamin A/C and lamin B1 levels in MG-63 cells. Representative microphotographs are also shown (bottom). BF- bright field, SSC- side scatter. (B) Protein plot generated by the Scansite program showing the full length of DNMT2/TRDMT1 protein and the predicted phosphorylation sites. (C) Table generated by Scansite program showing predicted site and sequence of DNMT2/TRDMT1 protein likely to be phosphorylated, possible factors causing post-translational modification and colocalization of the DNMT2/TRDMT1 with possible modifiers.

Therefore, we decided to predict whether the cytoplasmic and nuclear localization of DNMT2/TRDMT1 might be caused by post-translational modifications of DNMT2/TRDMT1. To test this, we used different bioinformatics tools, however, our interest focused on results obtained using the <http://scansite.mit.edu>. Scansite identifies short protein sequence motifs that are likely to be phosphorylated or mediate specific interactions with protein or phospholipid ligands [85]. Interestingly, high-resolution computational analysis revealed TRDMT1 as a potential phosphorylation target for ERK1 (MAPK3) at P361, PLCg (PLCG1) at Y266, and DNA-PK (PRKDC) at S327 (Fig. 4B and C). All predicted phosphorylation target sites are present in all isoforms studied. Furthermore, scanning analysis predicted DNMT2/TRDMT1 colocalization with PLCg in the cytoplasm, while with ERK1 and DNA-PK in

the nucleus (Fig. 4C). However, this analysis needs further validation using inhibitors and/or silencing of potential candidates.

In conclusion, we have shown for the first time that U-2 OS, SaOS-2, and MG-63 OS cell lines differ in the activity of proliferation-related signaling pathways, redox equilibrium, cell death pathways and DNA damage response. Moreover, we observed that MG-63 cells, which possess the highest levels of nuclear DNMT2/TRDMT1, exhibit the most abundant methylated RNA at the m<sup>5</sup>C position. Additionally, we hypothesize based on *in silico* analysis that the distinct cellular localization of DNMT2/TRDMT1 may be a result of post-translational modifications. Altogether, detailed characterization of three OS cell lines provided in the present study may be helpful for a better understanding of OS biology and identifying new targets for OS treatment.

### CRedit authorship contribution statement

**Gabriela Betlej:** Investigation, Visualization. **Tomasz Ząbek:** Methodology, Investigation. **Anna Lewińska:** Investigation, Writing – review & editing. **Dominika Błoniarczyk:** Investigation. **Iwona Rzeszutek:** Investigation, Writing – original draft, Visualization. **Maciej Wnuk:** Conceptualization, Methodology, Investigation, Writing – review & editing, Supervision, Funding acquisition.

### Declaration of Competing Interest

The authors declare the following financial interests/personal relationships which may be considered as potential competing interests: Maciej Wnuk reports financial support was provided by National Science Centre Poland.

### Acknowledgements

This research was funded by National Science Centre (Poland) OPUS grant UMO-2017/25/B/NZ2/01983 for M.W.

### Appendix A. Supplementary data

Supplementary data to this article can be found online at <https://doi.org/10.1016/j.jbo.2022.100448>.

### References

- [1] R.A. Durfee, M. Mohammed, H.H. Luu, Review of Osteosarcoma and Current Management, *Rheumatol. Ther.* 3 (2016) 221–243, <https://doi.org/10.1007/s40744-016-0046-y>.
- [2] A. Misaghi, A. Goldin, M. Awad, A.A. Kulidjian, Osteosarcoma: a comprehensive review, *SICOT-J.* 4 (2018) 12, <https://doi.org/10.1051/sicotj/2017028>.
- [3] L. Mirabello, R.J. Troisi, S.A. Savage, International osteosarcoma incidence patterns in children and adolescents, middle ages and elderly persons, *Int. J. Cancer.* 125 (2009) 229–234, <https://doi.org/10.1002/ijc.24320>.
- [4] F. Cersosimo, S. Lonardi, G. Bernardini, B. Telfer, G.E. Mandelli, A. Santucci, W. Vermi, E. Giurisato, Tumor-Associated Macrophages in Osteosarcoma: From Mechanisms to Therapy, *Int. J. Mol. Sci.* 21 (2020) 5207, <https://doi.org/10.3390/ijms21155207>.
- [5] X. Yu, J.T. Yustein, J. Xu, Research models and mesenchymal/epithelial plasticity of osteosarcoma, *Cell Biosci.* 11 (2021) 94, <https://doi.org/10.1186/s13578-021-00600-w>.
- [6] Y. Suehara, D. Alex, A. Bowman, S. Middha, A. Zehir, D. Chakravarty, L. Wang, G. Jour, K. Nafa, T. Hayashi, A.A. Jungbluth, D. Frosina, E. Slotkin, N. Shukla, P. Meyers, J.H. Healey, M. Hameed, M. Ladanyi, Clinical Genomic Sequencing of Pediatric and Adult Osteosarcoma Reveals Distinct Molecular Subsets with Potentially Targetable Alterations, *Clin. Cancer Res.* 25 (2019). 6346–6356. <https://doi.org/10.1158/1078-0432.CCR-18-4032>.
- [7] D. Wang, X. Niu, Z. Wang, C.L. Song, Z. Huang, K.N. Chen, J. Duan, H. Bai, J. Xu, J. Zhao, Y. Wang, M. Zhuo, X.S. Xie, X. Kang, Y. Tian, L. Cai, J.F. Han, T. An, Y. Sun, S. Gao, J. Zhao, J. Ying, L. Wang, J. He, J. Wang, Multiregion Sequencing Reveals the Genetic Heterogeneity and Evolutionary History of Osteosarcoma and Matched Pulmonary Metastases, *Cancer Res.* 79 (2019). 7–20. <https://doi.org/10.1158/0008-5472.CAN-18-1086>.
- [8] J.W. Martin, J.A. Squire, M. Zielenska, The Genetics of Osteosarcoma, *Sarcoma.* 2012. (2012). 627254. <https://doi.org/10.1155/2012/627254>.
- [9] S. Wilkesmann, J. Fellenberg, Q. Nawaz, B. Reible, A. Moghaddam, A. R. Boccaccini, F. Westhauser, Primary osteoblasts, osteoblast precursor cells or osteoblast-like cell lines: Which human cell types are (most) suitable for characterizing 45S5-bioactive glass? *J. Biomed. Mater. Res. A.* 108 (2020) 663–674, <https://doi.org/10.1002/jbm.a.36846>.
- [10] A. Keremu, A. Aini, Y. Maimaitirexiati, Z. Liang, P. Aila, P. Xierela, A. Tusun, H. Moming, A. Yusufu, Overcoming cisplatin resistance in osteosarcoma through the miR-199a-modulated inhibition of HIF-1 $\alpha$ , *Biosci. Rep.* 39 (2019). BSR20170080. <https://doi.org/10.1042/BSR20170080>.
- [11] J. Yang, Z. Ma, Y. Wang, Z. Wang, Y. Tian, Y. Du, W. Bian, Y. Duan, J. Liu, Necrosis of osteosarcoma cells induces the production and release of high-mobility group box 1 protein, *Exp. Ther. Med.* 15 (2017) 461–466, <https://doi.org/10.3892/etm.2017.5415>.
- [12] A.B. Mohseny, I. Machado, Y. Cai, K.-L. Schaefer, M. Serra, P.C.W. Hogendoorn, A. Llobart-Bosch, A.-M. Cleton-Jansen, Functional characterization of osteosarcoma cell lines provides representative models to study the human disease, *Lab. Invest.* 91 (2011) 1195–1205, <https://doi.org/10.1038/labinvest.2011.72>.
- [13] C. Pautke, M. Schieker, T. Fischer, A. Kolk, P. Neth, W. Mutschler, S. Milz, Characterization of osteosarcoma cell lines MG-63, Saos-2 and U-2 OS in comparison to human osteoblasts, *Anticancer Res.* 24 (2004) 3743–3748.
- [14] H. Bouterfa, A.R. Darlapp, E. Klein, T. Pietsch, K. Roosen, J.C. Tonn, Expression of different extracellular matrix components in human brain tumor and melanoma cells in respect to variant culture conditions, *J. Neurooncol.* 44 (1999) 23–33, <https://doi.org/10.1023/a:1006331416283>.
- [15] K.M. Niforou, A.K. Anagnostopoulos, K. Vougas, C. Kittas, V.G. Gorgoulis, G. T. Tsangaris, The proteome profile of the human osteosarcoma U2OS cell line, *Cancer Genomics Proteomics.* 5 (2008) 63–78.
- [16] L. Ottaviano, K.L. Schaefer, M. Gajewski, W. Huckenbeck, S. Baldus, U. Rogel, C. Mackintosh, E. de Alava, O. Myklebost, S.H. Kresse, L.A. Meza-Zepeda, M. Serra, A.M. Cleton-Jansen, P.C.W. Hogendoorn, H. Buerger, T. Aigner, H.E. Gabbert, C. Poremba, Molecular characterization of commonly used cell lines for bone tumor research: A trans-European EuroBoNet effort, *Genes. Chromosomes, Cancer.* 49 (2010) 40–51, <https://doi.org/10.1002/gcc.20717>.
- [17] L. Jiang, Y. Cui, J. Luan, X. Zhou, X. Zhou, J. Han, A comparative proteomics study on matrix vesicles of osteoblast-like Saos-2 and U2-OS cells, *Intractable Rare Dis. Res.* 2 (2013) 59–62, <https://doi.org/10.5582/irdr.2013.v2.2.59>.
- [18] S. Zhang, W. Guo,  $\beta$ -Elemene Enhances the Sensitivity of Osteosarcoma Cells to Doxorubicin via Downregulation of Peroxiredoxin-1, *OncoTargets Ther.* 14 (2021) 3599–3609, <https://doi.org/10.2147/OTT.S303152>.
- [19] H.C.A. Graat, M.A. Witlox, F.H.E. Schagen, G.J.L. Kaspers, M.N. Helder, J. Bras, G. R. Schaap, W.R. Gerritsen, P.L.J.M. Wuisman, V.W. van Beusechem, Different susceptibility of osteosarcoma cell lines and primary cells to treatment with oncolytic adenovirus and doxorubicin or cisplatin, *Br. J. Cancer.* 94 (2006) 1837–1844, <https://doi.org/10.1038/sj.bjc.6603189>.
- [20] Y. Mori, T. Shirai, R. Terauchi, S. Tsuchida, N. Mizoshiri, D. Hayashi, Y. Arai, T. Kishida, O. Mazda, T. Kubo, Antitumor effects of pristimerin on human osteosarcoma cells *in vitro* and *in vivo*, *OncoTargets Ther.* 10 (2017) 5703–5710, <https://doi.org/10.2147/OTT.S150071>.
- [21] K. Ye, S. Wang, J. Wang, H. Han, B. Ma, Y. Yang, Zebularine enhances apoptosis of human osteosarcoma cells by suppressing methylation of *ARHI*, *Cancer Sci.* 107 (2016) 1851–1857, <https://doi.org/10.1111/cas.13088>.
- [22] K. Filip, A. Lewinska, J. Adamczyk-Grochala, A. Marino Gammazza, F. Cappello, M. Lauricella, M. Wnuk, 5-Azacytidine Inhibits the Activation of Senescence Program and Promotes Cytotoxic Autophagy during Trdmt1-Mediated Oxidative Stress Response in Insulinoma  $\beta$ -TC-6 Cells, *Cells.* 11 (2022). 1213. <https://doi.org/10.3390/cells11071213>.
- [23] D. Błoniarczyk, J. Adamczyk-Grochala, A. Lewinska, M. Wnuk, The lack of functional *DNMT2/TRDMT1* gene modulates cancer cell responses during drug-induced senescence, *Aging.* 13 (2021) 15833–15874. <https://doi.org/10.18632/aging.203203>.
- [24] Q. Lan, P.Y. Liu, J.L. Bell, J.Y. Wang, S. Hüttelmaier, X.D. Zhang, L. Zhang, T. Liu, The Emerging Roles of RNA m6A Methylation and Demethylation as Critical Regulators of Tumorigenesis, Drug Sensitivity, and Resistance, *Cancer Res.* 81 (13) (2021) 3431–3440.
- [25] H. Chen, H. Yang, X. Zhu, T. Yadav, J. Ouyang, S.S. Truesdell, J. Tan, Y. Wang, M. Duan, L. Wei, L. Zou, A.S. Levine, S. Vasudevan, L. Lan, m5C modification of mRNA serves a DNA damage code to promote homologous recombination, *Nat. Commun.* 11 (2020) 2834, <https://doi.org/10.1038/s41467-020-16722-7>.
- [26] X. Zhu, X. Wang, W. Yan, H. Yang, Y. Xiang, F. Lv, Y. Shi, H. Li, L. Lan, Ubiquitination-mediated degradation of TRDMT1 regulates homologous recombination and therapeutic response, *NAR, Cancer.* 3 (2021) zcab010, <https://doi.org/10.1093/narcan/zcab010>.
- [27] G. Betlej, A. Lewinska, J. Adamczyk-Grochala, D. Błoniarczyk, I. Rzeszutek, M. Wnuk, Deficiency of TRDMT1 impairs exogenous RNA-based response and promotes retrotransposon activity during long-term culture of osteosarcoma cells, *Toxicol In Vitro.* 80 (2022), 105323, <https://doi.org/10.1016/j.tiv.2022.105323>.
- [28] A. Lewinska, J. Adamczyk-Grochala, A. Deregowska, M. Wnuk, Sulforaphane-Induced Cell Cycle Arrest and Senescence are accompanied by DNA Hypomethylation and Changes in microRNA Profile in Breast Cancer Cells, *Theranostics.* 7 (2017) 3461–3477, <https://doi.org/10.7150/thno.20657>.
- [29] A. Lewinska, D. Bednarz, J. Adamczyk-Grochala, M. Wnuk, Phytochemical-induced nuclear stress results in the inhibition of breast cancer cell proliferation, *Redox Biol.* 12 (2017) 469–482, <https://doi.org/10.1016/j.redox.2017.03.014>.
- [30] T. Koressaar, M. Remm, Enhancements and modifications of primer design program Primer3, *Bioinformatics.* 23 (2007) 1289–1291, <https://doi.org/10.1093/bioinformatics/btm091>.
- [31] A. Untergasser, I. Cutcutache, T. Koressaar, J. Ye, B.C. Faircloth, M. Remm, S.G. Rozen, Primer3—new capabilities and interfaces, *Nucleic Acids Res.* 40 (2012). e115. <https://doi.org/10.1093/nar/gks596>.
- [32] K.B. Nicholas, H.B. Nicholas, D.W. Deerfield, *GeneDoc: Analysis and visualization of genetic variation*, *EMBnet. News.* 4 (1997) 14.
- [33] C. Pfeffer, A. Singh, Apoptosis: A Target for Anticancer Therapy, *Int. J. Mol. Sci.* 19 (2018) 448, <https://doi.org/10.3390/ijms19020448>.
- [34] G.Y. Liou, P. Storz, Reactive oxygen species in cancer, *Free Radic. Res.* 44 (2010) 479–496, <https://doi.org/10.3109/10715761003667554>.
- [35] S.C. Gupta, D. Hevia, S. Patchva, B. Park, W. Koh, B.B. Aggarwal, Upsides and downsides of reactive oxygen species for cancer: the roles of reactive oxygen species in tumorigenesis, prevention, and therapy, *Antioxid. Redox Signal.* 16 (2012) 1295–1322, <https://doi.org/10.1089/ars.2011.4414>.
- [36] F.L. Sarmiento-Salinas, A. Perez-Gonzalez, A. Acosta-Casique, A. Ix-Ballote, A. Diaz, S. Trevino, N.H. Rosas-Murrieta, L. Millan-Perez-Pena, P. Maycotte, Reactive oxygen species: Role in carcinogenesis, cancer cell signaling and tumor progression, *Life Sci.* 284 (2021), 119942, <https://doi.org/10.1016/j.lfs.2021.119942>.
- [37] Q. Cui, J.Q. Wang, Y.G. Assaraf, L. Ren, P. Gupta, L. Wei, C.R. Ashby, D.H. Yang, Z. S. Chen, Modulating ROS to overcome multidrug resistance in cancer, *Drug Resist. Updat.* 41 (2018) 1–25, <https://doi.org/10.1016/j.drug.2018.11.001>.

- [38] C. Gorrini, I.S. Harris, T.W. Mak, Modulation of oxidative stress as an anticancer strategy, *Nat. Rev. Drug Discov.* 12 (2013) 931–947, <https://doi.org/10.1038/nrd4002>.
- [39] W. Liang, X. He, J. Bi, T. Hu, Y. Sun, Role of reactive oxygen species in tumors based on the 'seed and soil' theory: A complex interaction (Review), *Oncol. Rep.* 46 (2021) 208, <https://doi.org/10.3892/or.2021.8159>.
- [40] H. Maeda, T. Akaike, Nitric oxide and oxygen radicals in infection, inflammation, and cancer, *Biochemistry (Mosc.)* 63 (1998) 854–865.
- [41] R. Sullivan, C. Graham, Chemosensitization of Cancer by Nitric Oxide, *Curr. Pharm. Des.* 14 (2008) 1113–1123, <https://doi.org/10.2174/138161208784246225>.
- [42] V. Aggarwal, H. Tuli, A. Varol, F. Thakral, M. Yerer, K. Sak, M. Varol, A. Jain, M. d. Khan, G. Sethi, Role of Reactive Oxygen Species in Cancer Progression: Molecular Mechanisms and Recent Advancements, *Biomolecules*. 9 (2019) 735, <https://doi.org/10.3390/biom9110735>.
- [43] N. Koundouros, G. Poulogiannis, Phosphoinositide 3-Kinase/Akt Signaling and Redox Metabolism in Cancer, *Front. Oncol.* 8 (2018) 160, <https://doi.org/10.3389/fonc.2018.00160>.
- [44] S.H. Kim, K.Y. Kim, S.G. Park, S.N. Yu, Y.W. Kim, H.W. Nam, H.H. An, Y.W. Kim, S. C. Ahn, Mitochondrial ROS activates ERK/autophagy pathway as a protected mechanism against deoxydopodophyllotoxin-induced apoptosis, *Oncotarget*. 8 (2017) 111581–111596, <https://doi.org/10.18632/oncotarget.22875>.
- [45] J. Zhang, X.H. Yu, Y.G. Yan, C. Wang, W.J. Wang, PI3K/Akt signaling in osteosarcoma, *Clin. Chim. Acta.* 444 (2015) 182–192, <https://doi.org/10.1016/j.cca.2014.12.041>.
- [46] W. Zhang, J.C. Lee, S. Kumar, M. Gowen, ERK Pathway Mediates the Activation of Cdk2 in IGF-1-Induced Proliferation of Human Osteosarcoma MG-63 Cells, *J. Bone Miner. Res.* 14 (1999) 528–535, <https://doi.org/10.1359/jbmr.1999.14.4.528>.
- [47] R. Yang, S. Piperdi, R. Gorlick, Activation of the RAF/Mitogen-Activated Protein/Extracellular Signal-Regulated Kinase Kinase/Extracellular Signal-Regulated Kinase Pathway Mediates Apoptosis Induced by Chelerythrine in Osteosarcoma, *Clin. Cancer Res.* 14. (2008). 6396–6404, <https://doi.org/10.1158/1078-0432.CCR-07-5113>.
- [48] Y. Yu, F. Luk, J.L. Yang, W.R. Walsh, Ras/Raf/MEK/ERK pathway is associated with lung metastasis of osteosarcoma in an orthotopic mouse model, *Anticancer Res.* 31 (2011) 1147–1152.
- [49] Y.T. Wu, H.L. Tan, Q. Huang, C.N. Ong, H.M. Shen, Activation of the PI3K-Akt-mTOR signaling pathway promotes necrotic cell death via suppression of autophagy, *Autophagy*. 5 (2009) 824–834, <https://doi.org/10.4161/auto.9099>.
- [50] S. Cagnol, J.C. Chambard, ERK and cell death: mechanisms of ERK-induced cell death-apoptosis, autophagy and senescence, *FEBS J.* 277 (2010) 2–21, <https://doi.org/10.1111/j.1742-4658.2009.07366.x>.
- [51] W. Woessmann, X. Chen, A. Borkhardt, Ras-mediated activation of ERK by cisplatin induces cell death independently of p53 in osteosarcoma and neuroblastoma cell lines, *Cancer Chemother. Pharmacol.* 50 (2002) 397–404, <https://doi.org/10.1007/s00280-002-0502-y>.
- [52] A. Cazzaniga, J.A. Maier, S. Castiglioni, Prednisolone inhibits SaOS2 osteosarcoma cell proliferation by activating inducible nitric oxide synthase, *World, J. Transl. Med.* 5 (2016) 53–58, <https://doi.org/10.5528/wjtm.v5.i1.53>.
- [53] J.K. Lee, Y.L. Choi, M. Kwon, P.J. Park, Mechanisms and Consequences of Cancer Genome Instability: Lessons from Genome Sequencing Studies, *Annu. Rev. Pathol. Mech. Dis.* 11 (2016) 283–312, <https://doi.org/10.1146/annurev-pathol-012615-044446>.
- [54] D. Hanahan, R.A. Weinberg, Hallmarks of cancer: the next generation, *Cell*. 144 (2011) 646–674, <https://doi.org/10.1016/j.cell.2011.02.013>.
- [55] N. Hosoya, K. Miyagawa, Targeting DNA damage response in cancer therapy, *Cancer Sci.* 105 (2014) 370–388, <https://doi.org/10.1111/cas.12366>.
- [56] L.Q. Du, Y. Wang, H. Wang, J. Cao, Q. Liu, F.Y. Fan, Knockdown of Rad51 expression induces radiation- and chemo-sensitivity in osteosarcoma cells, *Med. Oncol.* 28 (2011) 1481–1487, <https://doi.org/10.1007/s12032-010-9605-1>.
- [57] P. Verma, R.L. Dilley, T. Zhang, M.T. Gyparaki, Y. Li, R.A. Greenberg, RAD52 and SLX4 act nonredundantly to ensure telomere stability during alternative telomere lengthening, *Genes Dev.* 33 (2019) 221–235, <https://doi.org/10.1101/gad.319723.118>.
- [58] Y. Zhang, L. Cai, R.X. Wei, H. Hu, W. Jin, X.B. Zhu, Different expression of alternative lengthening of telomere (ALT)-associated proteins/mRNAs in osteosarcoma cell lines, *Oncol. Lett.* 2 (2011) 1327–1332, <https://doi.org/10.3892/ol.2011.403>.
- [59] N. Arnoult, J. Karlseder, Complex interactions between the DNA-damage response and mammalian telomeres, *Nat. Struct. Mol. Biol.* 22 (2015) 859–866, <https://doi.org/10.1038/nsmb.3092>.
- [60] M. Lee, M. Hills, D. Conomos, M.D. Stutz, R.A. Dagg, L.M.S. Lau, R.R. Reddel, H. A. Pickett, Telomere extension by telomerase and ALT generates variant repeats by mechanistically distinct processes, *Nucleic Acids Res.* 42 (2014) 1733–1746, <https://doi.org/10.1093/nar/gkt1117>.
- [61] C.A. Lovejoy, W. Li, S. Reisenweber, S. Thongthip, J. Bruno, T. de Lange, S. De, J.H. J. Petrini, P.A. Sung, M. Jasin, J. Rosenbluh, Y. Zwang, B.A. Weir, C. Hatton, E. Ivanova, L. Maconail, M. Hanna, W.C. Hahn, N.F. Lue, R.R. Reddel, Y. Jiao, K. Kinzler, B. Vogelstein, N. Papadopoulos, A.K. Meeker, H.S. Scott, for the ALT Starr Cancer Consortium, Loss of ATRX, Genome Instability, and an Altered DNA Damage Response Are Hallmarks of the Alternative Lengthening of Telomeres Pathway, *PLoS Genet.* 8 (7) (2012) e1002772, <https://doi.org/10.1371/journal.pgen.1002772>.
- [62] Y. Hu, D. Bobb, J. He, D.A. Hill, J.S. Dome, The HSP90 inhibitor alvespimycin enhances the potency of telomerase inhibition by imetelstat in human osteosarcoma, *Cancer Biol. Ther.* 16 (2015) 949–957, <https://doi.org/10.1080/15384047.2015.1040964>.
- [63] R.L. Flynn, K.E. Cox, M. Jeitany, H. Wakimoto, A.R. Bryll, N.J. Ganem, F. Bersani, J.R. Pineda, M.L. Suvà, C.H. Benes, D.A. Haber, F.D. Boussin, L. Zou, Alternative lengthening of telomeres renders cancer cells hypersensitive to ATR inhibitors, *Science*. 347 (2015) 273–277, <https://doi.org/10.1126/science.1257216>.
- [64] T. Goncalves, G. Zoumpoulidou, C. Alvarez-Mendoza, C. Mancusi, L.C. Collopy, S. J. Strauss, S. Mittnacht, K. Tomita, Selective Elimination of Osteosarcoma Cell Lines with Short Telomeres by Ataxia Telangiectasia and Rad3-Related Inhibitors, *ACS Pharmacol. Transl. Sci.* 3 (2020) 1253–1264, <https://doi.org/10.1021/acspsci.0c00125>.
- [65] R.E. Verdun, J. Karlseder, The DNA Damage Machinery and Homologous Recombination Pathway Act Consecutively to Protect Human Telomeres, *Cell*. 127 (2006) 709–720, <https://doi.org/10.1016/j.cell.2006.09.034>.
- [66] A. Ho, F.R. Wilson, S.L. Peragine, K. Jeyanthan, T.R.H. Mitchell, X.-D. Zhu, TRF1 phosphorylation on T271 modulates telomerase-dependent telomere length maintenance as well as the formation of ALT-associated PML bodies, *Sci. Rep.* 6 (2016) 36913, <https://doi.org/10.1038/srep36913>.
- [67] M. Stagno D'Alcontres, A. Mendez-Bermudez, J.L. Foxon, N.J. Royle, P. Salomoni, Lack of TRF2 in ALT cells causes PML-dependent p53 activation and loss of telomeric DNA, *J. Cell Biol.* 179 (2007) 855–867, <https://doi.org/10.1083/jcb.200703020>.
- [68] A. Sfeir, T. de Lange, Removal of Shelterin Reveals the Telomere End-Protection Problem, *Science*. 336 (2012) 593–597, <https://doi.org/10.1126/science.1218498>.
- [69] K.E. Bohnsack, C. Höbartner, M.T. Bohnsack, Eukaryotic 5-methylcytosine (m<sup>5</sup>C) RNA Methyltransferases: Mechanisms, Cellular Functions, and Links to Disease, *Genes*. 10 (2019) 102, <https://doi.org/10.3390/genes10020102>.
- [70] X. Gu, H. Zhou, Q. Chu, Q. Zheng, J. Wang, H. Zhu, Uncovering the Association Between m<sup>5</sup>C Regulator-Mediated Methylation Modification Patterns and Tumour Microenvironment Infiltration Characteristics in Hepatocellular Carcinoma, *Front. Cell Dev. Biol.* 9 (2021), 727935, <https://doi.org/10.3389/fcell.2021.727935>.
- [71] Y. Chen, W. Yang, Y. Zhao, Y. Yang, Dynamic transcriptomic m<sup>5</sup>C and its regulatory role in RNA processing, *WIREs RNA*. 12 (2021) e1639.
- [72] A. Chellamuthu, S.G. Gray, The RNA Methyltransferase NSUN2 and Its Potential Roles in Cancer, *Cells*. 9 (2020) 1758, <https://doi.org/10.3390/cells9081758>.
- [73] S. Xue, H. Xu, Z. Sun, H. Shen, S. Chen, J. Ouyang, Q. Zhou, X. Hu, H. Cui, Depletion of TRDMT1 affects 5-methylcytosine modification of mRNA and inhibits HEK293 cell proliferation and migration, *Biochem. Biophys. Res. Commun.* 520 (2019) 60–66, <https://doi.org/10.1016/j.bbrc.2019.09.098>.
- [74] X. Han, M. Wang, Y.L. Zhao, Y. Yang, Y.G. Yang, RNA methylations in human cancers, *Seminars in Cancer Biology*. 75 (2021) 97–115, <https://doi.org/10.1016/j.semcancer.2020.11.007>.
- [75] Y. He, X. Yu, J. Li, Q. Zhang, Q. Zheng, W. Guo, Role of m<sup>5</sup>C-related regulatory genes in the diagnosis and prognosis of hepatocellular carcinoma, *Am. J. Transl. Res.* 12 (2020) 912–922.
- [76] L. Sun, W.K. Liu, X.W. Du, X.L. Liu, G. Li, Y. Yao, T. Han, W.Y. Li, J. Gu, Large-scale transcriptome analysis identified RNA methylation regulators as novel prognostic signatures for lung adenocarcinoma, *Ann. Transl. Med.* 8 (2020) 751, <https://doi.org/10.21037/atm-20-3744>.
- [77] Z. Huang, J. Pan, H. Wang, X. Du, Y. Xu, Z. Wang, D. Chen, Prognostic Significance and Tumor Immune Microenvironment Heterogeneity of m<sup>5</sup>C RNA Methylation Regulators in Triple-Negative Breast Cancer, *Front. Cell Dev. Biol.* 9 (2021), 657547, <https://doi.org/10.3389/fcell.2021.657547>.
- [78] M. Xue, Q. Shi, L. Zheng, Q. Li, L. Yang, Y. Zhang, Gene signatures of m<sup>5</sup>C regulators may predict prognoses of patients with head and neck squamous cell carcinoma, *Am. J. Transl. Res.* 12 (2020) 6841–6852.
- [79] A. Jeltsch, A. Ehrenhofer-Murray, T.P. Jurkowski, F. Lyko, G. Reuter, S. Ankr, W. Nellen, M. Schaefer, M. Helm, Mechanism and biological role of Dnmt2 in Nucleic Acid Methylation, *RNA Biol.* 14 (2017) 1108–1123, <https://doi.org/10.1080/15476286.2016.1191737>.
- [80] K. Rai, S. Chidester, C.V. Zavala, E.J. Manos, S.R. James, A.R. Karpf, D.A. Jones, B. R. Cairns, Dnmt2 functions in the cytoplasm to promote liver, brain, and retina development in zebrafish, *Genes Dev.* 21 (2007) 261–266, <https://doi.org/10.1101/gad.1472907>.
- [81] M. Schaefer, J.P. Steringer, F. Lyko, N. Hotchin, The *Drosophila* cytosine-5 methyltransferase Dnmt2 is associated with the nuclear matrix and can access DNA during mitosis, *PLoS One*. 3 (1) (2008) e1414, <https://doi.org/10.1371/journal.pone.0001414>.
- [82] D. Thiagarajan, R.R. Dev, S. Khosla, The DNA methyltransferase Dnmt2 participates in RNA processing during cellular stress, *Epigenetics*. 6 (2011) 103–113, <https://doi.org/10.4161/epi.6.1.13418>.
- [83] E. Urciuoli, V. D'Oria, S. Petrini, B. Peruzzi, Lamin A/C Mechanosensor Drives Tumor Cell Aggressiveness and Adhesion on Substrates With Tissue-Specific Elasticity, *Front. Cell Dev. Biol.* 9 (2021), 712377, <https://doi.org/10.3389/fcell.2021.712377>.
- [84] J. Zhang, Y. Ao, Z. Zhang, Y. Mo, L. Peng, Y. Jiang, Z. Wang, B. Liu, Lamin A safeguards the m<sup>5</sup>A methylase METTL14 nuclear speckle reservoir to prevent cellular senescence, *Aging Cell*. 19 (2020) e13215.
- [85] J.C. Obenauer, L.C. Cantley, M.B. Yaffe, Scansite 2.0: Proteome-wide prediction of cell signaling interactions using short sequence motifs, *Nucleic Acids Res.* 31 (2003) 3635–3641, <https://doi.org/10.1093/nar/gkg584>.